THE STAR FORMATION LAWS OF EDDINGTON-LIMITED STAR-FORMING DISKS

D. R. BALLANTYNE, J. N. ARMOUR AND J. INDERGAARD

Center for Relativistic Astrophysics, School of Physics, Georgia Institute of Technology, Atlanta, GA 30332; david.ballantyne@physics.gatech.edu

Accepted to The Astrophysical Journal

ABSTRACT

Two important avenues into understanding the formation and evolution of galaxies are the Kennicutt-Schmidt (KS) and Elmegreen-Silk (ES) laws. These relations connect the surface densities of gas and star formation (Σ_{gas} and $\dot{\Sigma}_*$, respectively) in a galaxy. To elucidate the KS and ES laws for disks where $\Sigma_{\mathrm{gas}} \gtrsim 10^4\,\mathrm{M}_\odot\,\mathrm{pc}^{-2}$, we compute 132 Eddington-limited star-forming disk models with radii spanning tens to hundreds of parsecs. The theoretically expected slopes (≈ 1 for the KS law and ≈ 0.5 for the ES relation) are relatively robust to spatial averaging over the disks. However, the star formation laws exhibit a strong dependence on opacity that separates the models by the dust-to-gas ratio that may lead to the appearance of a erroneously large slope. The total infrared luminosity (L_{TIR}) and multiple carbon monoxide (CO) line intensities were computed for each model. While L_{TIR} can yield an estimate of the average $\dot{\Sigma}_*$ that is correct to within a factor of 2, the velocity-integrated CO line intensity is a poor proxy for the average Σ_{gas} for these warm and dense disks, making the CO conversion factor (α_{CO}) all but useless. Thus, observationally derived KS and ES laws at these values of Σ_{gas} that uses any transition of CO will provide a poor measurement of the underlying star formation relation. Studies of the star formation laws of Eddington-limited disks will require a high-J transition of a high density molecular tracer, as well as a sample of galaxies with known metallicity estimates.

Subject headings: galaxies: evolution — galaxies: ISM — galaxies: starburst — stars: formation

1. INTRODUCTION

Galaxies can experience a wide variety of star formation phenomena, from the relative calm of star-forming regions beaded along a spiral arm, to the fury of a nuclear starburst burning through a trillion Suns. Yet, remarkably, the rate of star formation in such wildly disparate environments can be simply related to the density of gas in the star-forming region, $\dot{\Sigma}_* \propto \Sigma_{\mathrm{gas}}^N$, where $\dot{\Sigma}_*$ and Σ_{gas}, are the star formation rate (SFR) and total gas (i.e., atomic plus molecular) surface densities. This relation, known as the Kennicutt-Schmidt (KS) law, has been observed to hold over nearly four decades in Σ_{gas} with $N \approx 1.4$ (e.g., Schimdt 1959; Kennicutt 1998a,b; Yao et al. 2003; Kennicutt & Evans 2012), and is ultimately related to the efficiency of star formation and its connection to both local and global timescales (e.g., Elmegreen 1997; Silk 1997; Kennicutt 1998b; Elmegreen 2002; Krumholz & McKee 2005; Krumholz et al. 2009). The super-linear slope indicates that the star formation efficiency (i.e., the ratio of stellar mass formed to the gas mass in the star-forming region) increases at high densities. Measuring and understanding the KS law over a wide range of star-forming environments is crucial to elucidating comprehensive theories of star and galaxy formation (see discussion by Kennicutt & Evans 2012).

Most of the star formation in the universe occurred long ago at $z > 1$ when the majority of massive galaxies were being assembled (e.g., Hopkins & Beacom 2006; Pérez-González et al. 2008). With the advent of new sensitive millimeter arrays and detectors, the last decade has seen a significant advance in the study of the KS law at high redshifts (e.g., Daddi et al. 2010b; Genzel et al. 2010; Ivison et al. 2011; Freundlich et al. 2013; see Solomon & Vanden Bout (2005) and Carilli & Walter (2013) for reviews). Interestingly, these galaxies, which have both much larger star formation rates and gas densities than local objects, seem to follow a similar KS slope, but are vertically offset from the lo-

cal relation (Daddi et al. 2010b; Genzel et al. 2010) perhaps implying a fundamental difference in the stellar initial mass function (IMF) in the two regimes. However, many of these results rely on the assumption that the troublesome conversion factor $\alpha_{\mathrm{CO}} = \Sigma_{\mathrm{gas}}/I_{\mathrm{CO}}$ needed to convert from the observed CO velocity-integrated intensity, I_{CO}, to Σ_{gas} is bimodal with one value ($\alpha_{\mathrm{CO}} \approx 4$) for galaxies with Milky Way-like SFRs, and another value ($\alpha_{\mathrm{CO}} \approx 0.8$) for galaxies with much larger SFRs (i.e., high-z galaxies). When Narayanan et al. (2012) recently recomputed the KS law with a value of α_{CO} that varied continuously with I_{CO}, the relation was no longer bifurcated between the high and low-z galaxies and could be fit over a wide range in Σ_{gas} with $N \approx 2$ (see also Ostriker & Shetty 2011).

Alternatively, it has been argued (Elmegreen 1997; Silk 1997; Daddi et al. 2010b; Genzel et al. 2010) that a more fundamental star formation law is $\dot{\Sigma}_* \propto (\Sigma_{\mathrm{gas}}\Omega)^n$, where Ω is the orbital angular frequency in the star-forming region, usually estimated at the observed outer radius of a galaxy. Both high and low-z galaxies seem to follow this Elmegreen-Silk (ES) relation with $n \approx 1$, independent of the exact assumptions on α_{CO} (Daddi et al. 2010b; Genzel et al. 2010; although Narayanan et al. (2012) found that the scatter in the ES relation was reduced by using the continuously varying description of α_{CO}). In this formulation, a larger star-forming efficiency is found in rapidly star-forming galaxies because of occurring in more compact regions with shorter dynamical times.

Analysis and interpretation of the star formation laws at high redshift are hampered by gaps in the theory of star formation in galaxies at these redshifts. The interstellar medium of these galaxies are expected to be predominantly molecular (e.g., Solomon et al. 1997; Tacconi et al. 2010; Daddi et al. 2010a; Magdis et al. 2012) have gas fractions of several tens of percent (e.g., Geach et al. 2011; Swinbank et al. 2012; Narayanan et al. 2012b) with significant turbulence and large

pressures (e.g., Downes & Solomon 1998; Genzel et al. 2008; Wisnioski et al. 2011). Simulating this environment from first principles is computationally prohibitive, so analytical models have been developed that encompass many aspects of the physics in a well-defined region of parameter space (e.g., Thompson et al. 2005; Ostriker & Shetty 2011). In addition, as eluded to above, there may be severe uncertainties in relating the observed quantities (usually, infrared (IR) luminosity and CO intensity) to the physical parameters $\dot{\Sigma}_*$ and $\Sigma_{\rm gas}$ (e.g., Solomon & Vanden Bout 2005; Feldmann et al. 2012; Narayanan et al. 2012). Insofar as the IR luminosity captures the bolometric output of embedded star-forming regions, there are well known calibrations between the observed IR luminosity and SFR (e.g., Kennicutt 1998b; Rieke et al. 2009; Calzetti et al. 2010; Murphy et al. 2011). More problematic is how to convert from the line intensity of a molecule that comprises only a tiny fraction of the interstellar gas to an estimate of the entire gas mass. Although the CO lines are most commonly used due to its high abundance, it has been noted that because of their relatively low critical densities and high optical depth, they are likely very poor tracers of high density gas (e.g., Krumholz & Thompson 2007; Narayanan et al. 2008). Indeed, KS laws derived from a high density tracer such as HCN have produced a simple linear relation between $\dot{\Sigma}_*$ and $\Sigma_{\rm gas}$ for both high- and low-z galaxies (e.g., Gao & Solomon 2004a,b), although the conversion factor $\alpha_{\rm HCN}$ is just as uncertain as the one for CO (see the discussion by García-Burillo et al. 2012). Taken together, the combined uncertainties in both the existing theoretical framework and the observational conversions severely restrict the use of the KS or ES laws.

The most extreme star-forming regions are those with $\Sigma_{\rm gas} \gtrsim 10^4$ $M_\odot$ pc^{-2}. In this situation the opacity of the dense and dusty gas is so large that the ISM becomes optically thick in the IR, radiation pressure dominates over the turbulent pressure, and the disk is said to be Eddington-limited. Expected to occur in the cores (i.e., central few hundred pcs) of rapidly star-forming disks, these intense star-forming regions are difficult to investigate observationally, although evidence for such high values of $\Sigma_{\rm gas}$ have been recently inferred at the centers of some $z < 1$ post-starburst galaxies (Diamond-Stanic et al. 2012) and star-forming systems (García-Burillo et al. 2012). Their location also implies that these Eddington-limited star-forming disks may act as a 'bridge' between the black hole environment and the host galaxy, ferrying fuel through the disk toward the central black hole and potentially driving nuclear activity (Thompson et al. 2005; Ballantyne 2008). Thus, predictions of the observational signatures of Eddington-limited star-forming regions are needed to guide future observational studies of the centers of both active and inactive galaxies at all redshifts. Ostriker & Shetty (2011) analytically investigated star formation in environments with $10^2 \lesssim \Sigma_{\rm gas} \lesssim 10^4$ $M_\odot$ pc^{-2} when vertical pressure support is provided by supernova driven turbulence, and predicted that the KS law should have $N = 2$ (see also Thompson et al. 2005), in decent agreement with the high-z observations if one assumes that $\alpha_{\rm CO}$ is inversely correlated with $I_{\rm CO}$. In the Eddington-limited case the local KS law is expected to flatten to $N = 1$ (Thompson et al. 2005; Ostriker & Shetty 2011), but there have been no predictions for the ES law nor work on how clearly these laws will translate for an observation that encompasses an entire > 100 pc star-forming disk and contains a significantly variable SFR

and $\Sigma_{\rm gas}$. In this paper we use the Thompson et al. (2005) model of an Eddington-limited disk to self-consistently calculate the radial structure of over 100 nuclear star-forming disks, and, through the use of CO radiative transfer calculations, we investigate the relationship between observable (L_{IR} and I_{CO}) and physical ($\dot{\Sigma}_*$ and $\Sigma_{\rm gas}$) variables in these most extreme star-forming environments.

The next section describes the Eddington-limited star-forming disk model, the calculation of our model database, and the CO radiative transfer method. Both the KS and ES star formation laws predicted by these models are presented in Section 3. The observational star formation law (the IR-CO relationship) that is predicted by these models and its relationship to the physical KS and ES laws is described in Section 4. A discussion and concluding remarks are presented in Section 5. Throughout this paper the *total infrared luminosity* ($L_{\rm TIR}$) is defined as the 3–1100 μm luminosity (Murphy et al. 2011), and helium is not accounted for in $\Sigma_{\rm gas}$ or $\alpha_{\rm CO}$. Unless otherwise specified all CO intensities or luminosities refer to the $J = 1 - 0$ rotational transition.

2. CALCULATIONS

2.1. *The Eddington-Limited Star-Forming Disk Model*

The Eddington-limited starburst disk model utilized here was developed by Thompson et al. (2005), and a short summary of the relevant details is presented below (see also Thompson 2009).

Star formation is modeled simply as an energy source at a location r within a one-dimensional single phase medium that rotates with angular frequency Ω in the potential of a galactic bulge (modeled as an isothermal sphere) with dispersion σ and central black hole of mass $M_{\rm BH}$ (these two quantities are assumed to be related by $M_{\rm BH} = 2 \times 10^8 (\sigma/200$ km s$^{-1})^4$ $M_\odot$; e.g., Tremaine et al. 2002). Gas, radiation and turbulent pressure driven by supernova all combine to provide the vertical support against gravity:

$$p_{\rm gas} + \epsilon \dot{\Sigma}_* c \left(\frac{\tau_V}{2} + \xi \right) = \rho h^2 \Omega^2, \qquad (1)$$

where $p_{\rm gas} = \rho k T / m_{\rm p}$, and $\rho h^2 \Omega^2$ is the total pressure required for hydrostatic balance in the bulge potential (with h denoting the gas scale height and ρ indicating the gas density of the star-forming disk; the self-gravity of the disk is neglected here). Thompson et al. (2005) show that in the optically thick limit the radiation pressure is $\epsilon \dot{\Sigma}_* c \tau_V / 2$ where ϵ is the IMF-dependent efficiency between SFR and luminosity (i.e., $L = \epsilon \dot{M}_* c^2$, where $\dot{M}_*$ is the local SFR) and $\tau_V = \kappa \Sigma_{\rm gas}/2$ is the vertical optical depth in the IR ($\kappa(T, \rho)$ is the Rosseland mean opacity of the dusty gas at temperature T and density ρ). The turbulent pressure driven by supernova can also be written as proportional to the local SFR density, $\epsilon \xi \dot{\Sigma}_* c$, where $\xi \approx 1$ (Thompson et al. 2005). From above, a rms speed c_s can be defined using the total pressure as $c_s = h\Omega$, where it is understood that gas, radiation and turbulent pressure all contribute to this rms speed. As described below, the models studied in this paper all have a radially-averaged $\tau_V > 1$ and are thus dominated by radiation pressure for almost all radii.

The star-forming disk is assumed to be always just unstable to gravitational instabilities; that is, Toomre's Q parameter is set equal to one. Material with gas fraction $f_{\rm gas}$ is fed onto to the disk at a radius $r_{\rm out}$ from the black hole, and, through a

hypothesized global torque (provided by, e.g., a spiral instability or a bar; Goodman 2003; Englmaier & Shlosman 2004; Maciejewski 2004), can slowly accrete towards the center with a radial velocity equal to a fixed fraction m of the local rms speed (Goodman 2003), i.e., $\dot{M} = 2\pi r \Sigma_{gas} m c_s$. At any radius r, Thompson et al. (2005) showed that $\dot{M}$ and f_{gas} can be related through

$$f_{\rm gas} = \left(\frac{2^{3/2} \dot{M} G}{Q m \Omega^3 r^3} \right)^{1/2}. \qquad (2)$$

As the gas moves through the disk, it is also producing stars at a rate of $\dot{\Sigma}_*$, which, in the optically thick limit, is determined by requiring radiation pressure in the IR to support the disk (eq. 1) as well as $Q = 1$:

$$\dot{\Sigma}_* = \frac{\sqrt{2} f_{\rm gas} Q \sigma^2}{\epsilon \kappa c r}, \qquad (3)$$

where r is assumed to be large enough that the black hole potential is negligible. The star formation slowly consumes the gas as r decreases, reducing both $\dot{M}$ and f_{gas}, i.e.,

$$\dot{M} = \dot{M}_{\rm out} - \int_{r_{\rm out}}^{r} 2\pi r' \dot{\Sigma}_* dr', \qquad (4)$$

where $\dot{M}_{\rm out}$ is the mass accretion onto the disk at r_{out}. However, the $Q = 1$ assumption causes a rising density in the inner regions of the disk that substantially increases τ_V so that even a moderately increasing $\dot{\Sigma}_*$ can still support the disk through radiation pressure. The solution at radius r is determined by finding the minimum central gas temperature T and associated κ to ensure vertical pressure balance, either through the sum of gas and turbulent pressure, or, if there is enough star formation, radiation pressure. Eventually, either the gas available for star formation becomes too small to maintain $Q = 1$, or energy release through gas accretion pushes $Q > 1$, and the calculation ceases.

Substituting eq. 2 into eq. 3 results in predictions for both the ES and KS laws in the disks:

$$\dot{\Sigma}_* = \left(\frac{2^{3/2} \pi Q G}{\epsilon^2 c^2} \frac{c_s}{\kappa^2} \Sigma_{\rm gas} \Omega \right)^{1/2} \qquad (5)$$

and, using Q to eliminate Ω (see Thompson et al. 2005, eq. 3),

$$\dot{\Sigma}_* = \left(\frac{2^{1/2} \pi Q G}{\epsilon c \kappa} \right) \Sigma_{\rm gas}. \qquad (6)$$

These equations have to be viewed carefully because, as seen in eq. 4, Σ_{gas} is not an independent variable; its value at some radius r will depend on $\dot{\Sigma}_*$ at larger radii. As seen in Sect. 3, this property may affect the predicted slopes of the star formation laws. In sum, radiation pressure supported star-forming disks predict a KS relation with $N \approx 1$, and an ES law with $n \approx 0.5$. Of course, both of these predictions rely on the assumptions that $Q = 1$ and the disk is optically thick in the IR and therefore radiation pressure supported.

In order to determine how these laws will manifest in observational surveys of several galaxies, the full disk models need to be calculated over a wide range of parameters. There are five input parameters for each model: the black hole mass $M_{\rm BH}$ (which determines σ), the angular momentum parameter m, the outer radius $r_{\rm out}$, the gas fraction at the

outer radius $f_{\rm gas}$, and a dust-to-gas multiplicative factor for the opacity to account for the enhanced metallicity observed in the centers of galaxies (e.g., Muñoz-Mateos et al. 2009). As in Thompson et al. (2005), the Semenov et al. (2003) calculation of the Rosseland mean opacity for dusty interstellar gas is used for all models. Calculations are performed for each permutation of $\log(M_{\rm BH}/{\rm M}_\odot) = 7, 7.5, 8, 8.5$, $m = 0.0075, 0.01, 0.025, 0.05, 0.075, 0.1, 0.2$, $r_{\rm out} = 50, 100, 150, 200, 250\,{\rm pc}$, $f_{\rm gas} = 0.1, 0.5, 0.9$ and dust-to-gas ratios equal to $1\times$, $5\times$ and $10\times$ the local ISM value, resulting in a suite of 1260 models. While the models are limited to $r_{\rm out} \leq 250$ pc, the results on the star-formation laws do not depend on this size (as is seen for the observed KS and ES laws), and are valid for any Eddington-limited star-forming region. The range of input gas fractions is consistent with the observed estimates (e.g., Tacconi et al. 2010; Magdis et al. 2012) that show an increase to $\sim$50% at $z \sim 2$ (the $f_{\rm gas}$ input to the model drops steadily through the disk as the star formation uses up the available gas; eqs. 2 & 4). We employ a a standard Kroupa/Salpeter IMF with $\alpha_{\rm IMF} = -2.35$ (Salpeter 1955; Kroupa & Weidner 2003) between 1 and 100 M$_\odot$ and $\alpha_{\rm IMF} = -1.3$ between 0.1 and 1 M$_\odot$ (where the number of stars with masses between M and $M + dM$ is proportional to $M^{\alpha_{\rm IMF}}$). This IMF is then input into a Starburst99 stellar synthesis model (Leitherer et al. 1999) to compute the bolometric luminosity of a stellar population with a constant SFR and with the given IMF as a function of time. The value of $\epsilon = L/\dot{M}c^2$ is then measured at an age of 10^8 yr yielding $\epsilon = 7.1 \times 10^{-4}$ (very similar to value of 6.2×10^{-4} used by Ostriker & Shetty 2011)[1].

As described in detail by Thompson et al. (2005), roughly two different types of star-forming disks result from this theoretical description. In about one-third of the models the gas maintains a large optical depth over the entire disk, resulting in the temperature in the inner parsec of the disk exceeding the dust sublimation temperature and causing a significant burst of star formation in order to maintain $Q = 1$. These parsec-scale bursts could puff up the disk, and, if they do not use up all the gas, may both fuel and obscure the central black hole. The observational properties of these disks have been studied elsewhere (Ballantyne 2008; Armour & Ballantyne 2012), and, as they are not directly related to the study of general star-forming galaxies, the description of their star formation laws are deferred to later paper. The remaining models reach the maximum SFR, SFR$_{\rm max}$, at $r_{\rm out}$ with the SFR declining toward smaller r. Many of these disks are actually gas-pressure dominated or do not extend very far before $\dot{\Sigma}_*$ becomes too small to maintain $Q = 1$. As our interest here is studying radiation pressure dominated star-forming disks that can extend tens to hundreds of parsecs, we selected only models with a radially-averaged $\tau_V > 1$ and an inner radius $< 0.04 r_{\rm out}$ for further investigation (including less extended disks only in-

---

[1] The assumption of $Q = 1$ and the location of the star formation in the galactic nucleus results in significant gas densities with ρ rising from $\sim 10^{-20}$ g cm^{-3} (148 M$_\odot$ pc^{-3}) to $\gtrsim 10^{-14}$ g cm^{-3} (1.48×10^8 M$_\odot$ pc^{-3}). Recently, Kroupa et al. (2012) argued that there is a density and metallicity dependence to the IMF and proposed that the IMF slope above ≈ 1 M$_\odot$ flattens to one that depends on density, $\alpha_{\rm IMF} = -1.86 + 0.43 \log(\rho/10^6 {\rm M}_\odot \, {\rm pc}^{-3})$ when $\rho > 9.5 \times 10^4$ M$_\odot$ pc^{-3}. To test the observational consequences of this IMF, the suite of 1260 models run with the traditional Kroupa-Salpeter IMF was re-run with a top-heavy IMF $\alpha_{\rm IMF} = -1.86$ between 1 and 100 M$_\odot$. This IMF yields $\epsilon = 1.5 \times 10^{-3}$. There were no qualitative differences in any of the results of this paper between the two IMFs.
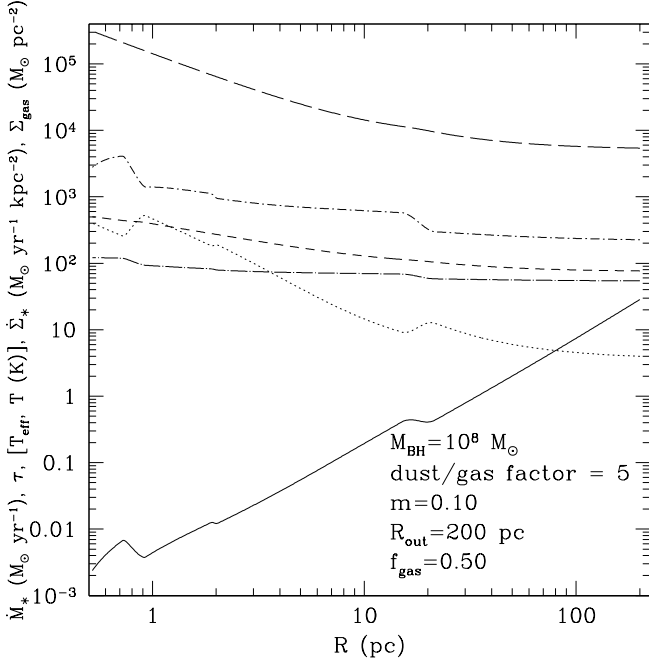
Figure 1. Several properties of an example Eddington-limited star-forming disk calculated using the theory described in section 2.1 including the SFR (solid line), the vertical optical depth in the IR τ (dotted line), the effective temperature $T_{\rm eff}$ (dot-long-dashed line), the central temperature T (short dashed line), the star formation surface density $\dot{\Sigma}_*$ (dot-short-dashed line), and the gas surface density $\Sigma_{\rm gas}$ (long dashed line).

creases the scatter of the derived relations). This selection criteria yields 132 model star-forming disks. Figure 1 shows several of the properties of one of these Eddington-limited star-forming disks. The plot clearly shows the implications of fixing $Q = 1$: the increasing $\Sigma_{\rm gas}$ keeps τ_V large enough so that radiation pressure dominates over nearly 200 pc. This fact, in turn, keeps the disk very warm with temperatures $T > 100$ K and $\dot{\Sigma}_* \sim 10^3$ $\rm M_\odot$ $\rm yr^{-1}$ $\rm kpc^{-2}$.

Figure 1 illustrates that the quantities that enter into the star formation laws (i.e., SFR, $\dot{\Sigma}_*$ and $\Sigma_{\rm gas}$) can vary dramatically over the size of the star-forming disk. As these variations will be unresolved at most redshifts, we consider both the radial average and the mass-weighted average of these variables when constructing the predicted KS and ES laws. For example, the mass-weighted average of the SFR along the disk, $\langle {\rm SFR} \rangle_{mw}$, is calculated as follows:

$$\langle {\rm SFR} \rangle_{mw} = \frac{\sum (2\pi r \Delta r \Sigma_{\rm gas}(r)/f_{\rm gas}(r)){\rm SFR}(r)\,\Delta r}{\sum (2\pi r \Delta r \Sigma_{\rm gas}(r)/f_{\rm gas}(r))\,\Delta r},$$

(7)

where $\Sigma_{\rm gas}/f_{\rm gas}$ is the total dynamical mass surface density. The simple radial average, $\langle {\rm SFR} \rangle$, is computed as in Eq. 7 but with the $(2\pi r \Delta r \Sigma_{\rm gas}/f_{\rm gas})$ factors omitted.

Finally, it is important to bear in mind the limitations associated with this model including the lack of any clumpiness which is found by hydrodynamical simulations of turbulence supported disks (e.g., Shetty & Ostriker 2012). In addition, as these disks are Eddington-limited they will may be subject to Rayleigh-Taylor instabilities (Krumholz & Thompson 2012), and could also drive outflows and feedback matter and energy into the galaxy (Murray et al. 2005; Andrews & Thompson 2011). The effects of outflows on the structure of these disks

is not considered here. Feedback from an accreting black hole is also not treated, so comparisons between the predictions and data should be limited to sources without active nuclei. It is expected that the impact of these limitations will be mostly offset by considering radially averaged quantities, a wide range of model parameters, and by comparing to constraints derived from observations of many dozens of individual galaxies.

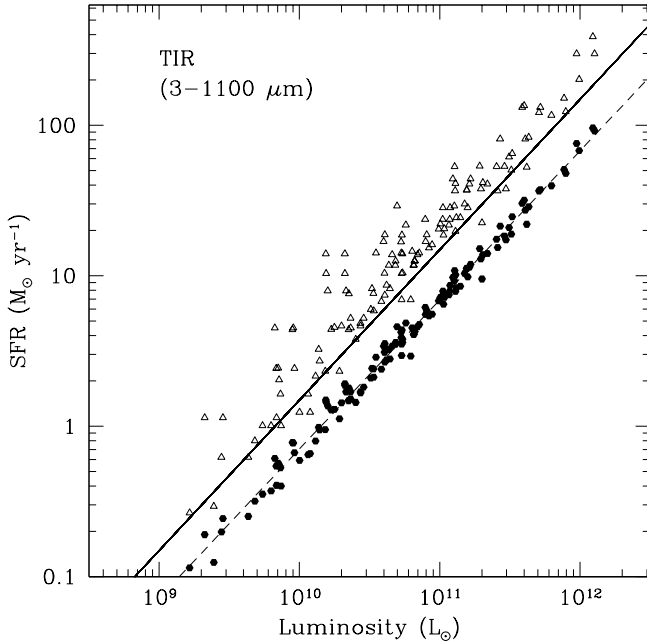## 2.2. *Infrared Luminosity and SFR*

The SFR is one of the most important observational properties of a galaxy as it gives crucial information on the galaxy's gas content and evolutionary state. Estimating the SFR typically relies on utilizing one of a number of relationships between SFR and the luminosity of the galaxy in a specific wavelength or energy range (Kennicutt & Evans 2012). As most of the starlight produced in high-z star-forming galaxies is absorbed by dust and re-emitted in the IR, the SFR-$L_{\rm TIR}$ relationship determined by Kennicutt (1998b) and Murphy et al. (2011) is one of the most frequently used SFR estimators, as well as serving as the calibration for SFR estimates at single IR wavelengths (Rieke et al. 2009; Calzetti et al. 2010). As described by Kennicutt (1998b) and Murphy et al. (2011), the SFR-$L_{\rm TIR}$ relationship was calculated using Starburst99 models assuming that 100% of the bolometric luminosity of a stellar population with a constant SFR is captured and emitted in the IR. This scenario is also fulfilled by the optically thick star-forming disk models with $\langle \tau_V \rangle > 1$, as τ_V is the vertical optical depth in the IR. Thus, as the SFR is known throughout each disk, it is interesting to determine how accurately the Murphy et al.-derived SFRs describe the star-forming properties of the model disks.

Since these disks are largely optically thick at all radii, the effective temperature $T_{\rm eff}$ of one side of the disk surface at radius r is related to half of the total flux produced by star formation: $\sigma_{\rm SB}T_{\rm eff}^4 = (1/2)\epsilon\dot{\Sigma}_* c^2$, where $\sigma_{\rm SB}$ is the Stefan-Boltzmann constant (Thompson et al. 2005). Assuming that each annulus of the disk radiates as a blackbody and is viewed face-on, the IR spectral energy distribution (SED) of each model is calculated as

$$\lambda L_\lambda = \frac{2\pi hc^2}{\lambda^4} \int_{r_{in}}^{r_{out}} \frac{2\pi r dr}{\exp[hc/\lambda k_{\rm B} T_{\rm eff}(r)] - 1},$$

(8)

where r_{in} is the inner radius for each model, h is Planck's constant and $k_{\rm B}$ is Boltzmann's constant. The $L_{\rm TIR}$ for each model is then computed by integrating the SED from 3–1100 μm. This luminosity can then be compared to various calculations of the disk SFR, such as $\langle {\rm SFR} \rangle$, ${\rm SFR}_{\rm max}$, and $\langle {\rm SFR} \rangle_{mw}$.

Figure 2 plots the Murphy et al. (2011) calibration $(\log({\rm SFR}/{\rm M}_\odot\ {\rm yr}^{-1}) = \log(L_{\rm TIR}/{\rm erg\ s}^{-1}) - 43.41)$ as the solid line, ${\rm SFR}_{\rm max}$ versus $L_{\rm TIR}$ (open triangles), and $\langle {\rm SFR} \rangle$ against $L_{\rm TIR}$ (solid points). The ${\rm SFR}_{\rm max}$, $\langle {\rm SFR} \rangle$ and $L_{\rm TIR}$ are derived directly from the models as described above. Evidently, the Murphy et al. (2011) calormetric relation provides a coarse approximation to the maximum SFR of each disk. This is a natural consequence of the assumption of a single SFR that underlies the original computation of the SFR-$L_{\rm TIR}$ relationship. The maximum SFR in the disk provides the largest contribution to the luminosity, so the estimated SFR from the $L_{\rm TIR}$ relationships will be closest to the maximum rate. However, as shown in Fig. 2, a better (with $\sim 10\times$ smaller scatter) SFR-$L_{\rm TIR}$ relationship is found with

Figure 2. Radially averaged (filled circles) and maximum (open triangles) SFRs from Eddington-limited star-forming disks plotted as a function of the infrared luminosity (computed from the spectrum derived from eq. 8). The short dashed line denotes the least-squares fit to the data while the solid line plots the SFR calibration published by Murphy et al. (2011).

the $\langle \text{SFR} \rangle$ which is, on average, 2.2 ± 0.3 smaller than the values predicted by the Murphy et al. (2011) calibration at the same luminosity. A least squares fit to the $\langle \text{SFR} \rangle$-$L_{\text{TIR}}$ relationship (dashed line) yields $\log(\langle \text{SFR} \rangle / \text{M}_\odot \ \text{yr}^{-1}) = (0.991 \pm 0.008) \log(L_{\text{TIR}}/\text{L}_\odot) - (10.07 \pm 0.09)$. Thus, the $\langle \text{SFR} \rangle$ is used throughout the paper to quantify the SFR for any particular model.

2.3. *Computing the CO Line Emission*

The CO intensity for multiple rotational lines is computed for each model using the one-dimensional version of the molecular line radiative transfer code RATRAN (Hogerheijde & van der Tak 2000). Armour & Ballantyne (2012) previously used RATRAN to study the CO spectral line energy distributions (SLEDs) of eighteen star-forming disk models (nine with a pc-scale burst and nine without), and a complete description of the calculation procedure is described in that paper. Below is a summary of the key parameters and assumptions that enter into the calculation.

The temperature and density of the star-forming disk models are computed on a logarithmic radial grid which is input into RATRAN. As mentioned above the Eddington-limited star-forming disks are uniformly very dense, so that the gas is expected to be entirely molecular as long as $T \lesssim 1000$ K (e.g., Pelupessy et al. 2006). Thus, the molecular fraction of the gas is set to unity for all radii, and the CO abundance is set to be 10^{-4} of the gas number density (Klemperer 2006). Since the star-forming gas is under high pressure and typically has densities $> 10^4$ cm^{-3}, gas and dust will be well mixed, and the molecular kinetic temperature and dust temperatures are set to the central temperature T (Goldsmith 2001). Dust opacity is included in the radiative transfer calculation with a temperature dependent broken power-law opacity (see Armour & Ballantyne 2012), and is scaled as appropriate for

each model's dust-to-gas factor. The turbulent line width at each radius is derived from the local rms speed c_s (i.e., the Doppler broadening parameter is $b = (2\sqrt{\ln(2)})^{-1} c_s$), and the radial velocity is mc_s, as defined above. Once RATRAN completes the radiative transfer calculation for a disk model, the Miriad software package (Sault et al. 1995) is used to remove the appropriate dust emission from each spectral line and integrate over velocity to produce the velocity-integrated intensity I_{CO} in K km s^{-1}. Using this method, CO line intensities for the $J =$1–0, 2–1, 3–2, 4–3, 5–4, 6–5, 7–6, 8–7 and 9–8 transitions are predicted for each Eddington-limited star-forming disk model.

3. THE STAR FORMATION LAWS
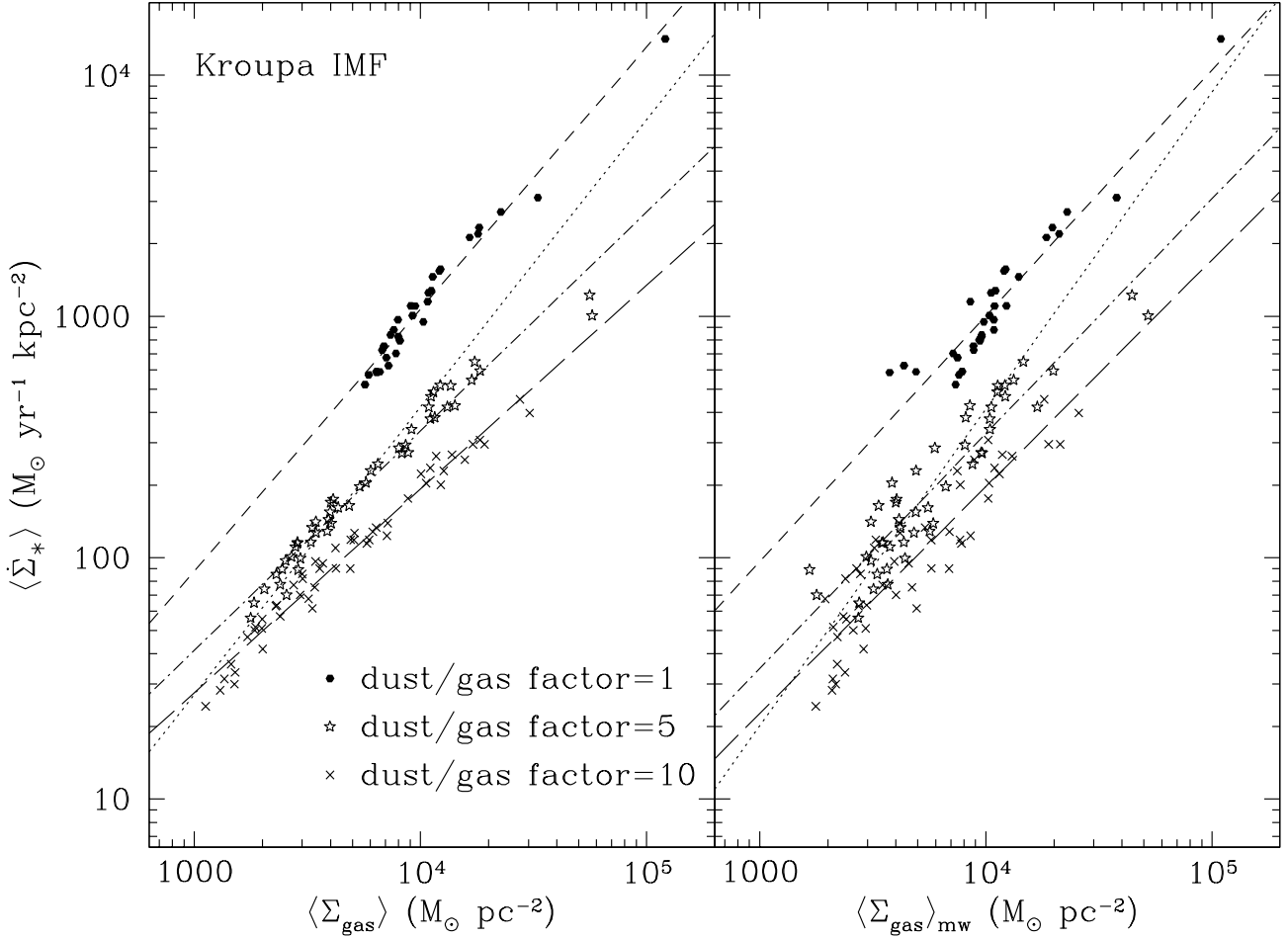
3.1. *The Kennicutt-Schmidt Relation*

Turning now to the star formation laws predicted by the Eddington-limited star-forming disks, Figure 3 plots the KS law in two ways: $\langle \dot{\Sigma}_* \rangle$ versus $\langle \Sigma_{\text{gas}} \rangle$ (left panel) and $\langle \dot{\Sigma}_* \rangle$ against $\langle \Sigma_{\text{gas}} \rangle_{mw}$ (right panel). The theoretical expectation is for $\dot{\Sigma}_* \propto \Sigma_{\text{gas}}/\kappa$ (Eq. 6), and, indeed, we find that the KS laws, calculated from these radial averages, have slopes close to unity and are seperated vertically by the dust-to-gas enhancement factor (that increases κ). The scatter in the KS relations is smallest when plotted against $\langle \Sigma_{\text{gas}} \rangle$ because the same spatial averaging is being performed on both quantities. However, due to the dependence of Σ_{gas} on $\dot{\Sigma}_*$ (see eq. 4 and surrounding discussion), the slopes of the KS laws in the left-hand panel can drift away from the expectation of $N = 1$. This effect is enhanced for larger dust-to-gas enhancement factors because a larger κ reduces $\dot{\Sigma}_*$ and thus Σ_{gas} does not decrease as fast with radius. The spatial averaging therefore results in a larger Σ_{gas} which then flattens the slope of the relations. By plotting the quanitites with different spatial averaging, the right-hand panel breaks the dependence of Σ_{gas} on $\dot{\Sigma}_*$ and shows that indeed the KS laws follow the theoretical expectation with $N \approx 1$.

A random selection of galaxies will likely exhibit a wide range of dust-to-gas ratios that may be difficult to observationally seperate. The dotted lines in Fig. 3 plot the KS relations found when including all the model points, regardless of the dust-to-gas factor. The resulting slopes are $N = 1.2$ and 1.3 for the $\langle \Sigma_{\text{gas}} \rangle$ and $\langle \Sigma_{\text{gas}} \rangle_{mw}$ panels, respectively. These values are very similar to the observed KS laws (e.g., Kennicutt & Evans 2012), and indicate that the common practice of measuring the KS relation by compiling a large collection of heterogeneous data may be hiding important clues of the physics of star-forming disks. Future investigations of the star formation laws may benefit from the analysis of a smaller sample of galaxies with well known properties.

3.2. *The Elmegreen-Silk Relation*

The ES law predicted from the radiation pressure dominated star-forming disk models are shown in Fig. 4, with the same symbols and line styles as the previous KS law figure. Following the current observational practice the orbital frequency is set to the inverse of the dynamical timescale at r_{out}, i.e., $\tau_{\text{dyn}} = 1/\Omega(r_{\text{out}})$. The theoretical expectation for the ES law is $\dot{\Sigma}_* \propto (\Sigma_{\text{gas}}\Omega/\kappa^2)^{0.5}$ (eq. 5), which is in good agreement with the relations seen in Fig. 4. There is a flattening of the slope with the dust-to-gas enhancement factor that is reduced in the $\langle \Sigma_{\text{gas}} \rangle_{mw}/\tau_{\text{dyn}}$ plot. The explanation for this effect

Figure 3. Kennicutt-Schmidt relations, defined either as $\langle\dot{\Sigma}_*\rangle$ vs. $\langle\Sigma_{\mathrm{gas}}\rangle$ (left panel) or as $\langle\dot{\Sigma}_*\rangle$ vs. $\langle\Sigma_{\mathrm{gas}}\rangle_{mw}$ (right panel), predicted by the Eddington-limited starburst disk models. The slope of the relations are slightly dependent on the dustiness of the gas with $N = 1.1, 0.91$ and 0.84 when plotted versus $\langle\Sigma_{\mathrm{gas}}\rangle$ and a dust-to-gas enhancement of $1\times, 5\times$ and $10\times$, respectively. When $\langle\dot{\Sigma}_*\rangle$ is plotted against $\langle\Sigma_{\mathrm{gas}}\rangle_{mw}$ the slopes are $N = 1.0, 0.97$ and 0.94 as the dustiness of the gas increases. The dotted line in each panel plots the relation when all models are considered, irrespective of the dust-to-gas factor. In that case, $N = 1.2$ (left panel) and 1.3 (right panel), very similar to the KS relations measured from less intense star-forming regions at low and high redshift (e.g., Kennicutt & Evans 2012).

is the same as with the KS relations discussed above. However, it is clear from a comparison of figs. 3 and 4 that the ES law has significantly more scatter than the KS relations (about a $3\times$ larger rms in the $\langle\Sigma_{\mathrm{gas}}\rangle$ plots; $\sim 50\%$ larger rms in the $\langle\Sigma_{\mathrm{gas}}\rangle_{mw}$ panels). This increased scatter is likely due to dividing a radial average by the orbital time at one radius, as well as a contribution due to variations in the rms speed in each model (eq. 5). It is notable that even when all the models are fit with a powerlaw, irrespective of the dust-to-gas factor, the measured slopes ($n = 0.70$ and 0.73) are still significantly sub-linear. Thus, measurements of a sub-linear ES-law in high-z star-forming galaxies may provide compelling evidence for a high-density Eddington limited environment.

4. THE INFRARED–CO RELATIONSHIP AND THE OBSERVED STAR FORMATION LAWS

The previous section described the theoretical expectations for the star formation laws governing the radiation pressure supported disks. To test the theory, these laws must be observationally inferred from data of a sample of galaxies, which,

at high-z, are typically limited to photometric measurements such as an IR luminosity and a molecular line intensity. The challenge is then to turn these measured quantities into accurate estimates of $\dot{\Sigma}_*$ and Σ_{gas} for each galaxy. In this section, we make use of our predicted IR luminosities and I_{CO} for each disk model[2] to test how well the observationally derived star formation laws recover the theoretical laws presented in Sect. 3.

Since an IR luminosity is correlated with the SFR (Sect. 2.2) and the molecular line intensity is connected *in some manner* to the total gas content of galaxy, a common zeroth-order measurement of the KS law is made by plotting the observed IR luminosity against a molecular line luminosity or intensity (Figure 5). The CO $J = 1 - 0$ transition is used as the molecular line tracer in this plot because it is one of the most commonly measured lines; however, the densities and temperatures of these disks are large enough that

---

[2] We work with the velocity integrated intensity I_{CO} instead of L'_{CO} to more closely match the observables expected for high-z galaxies.
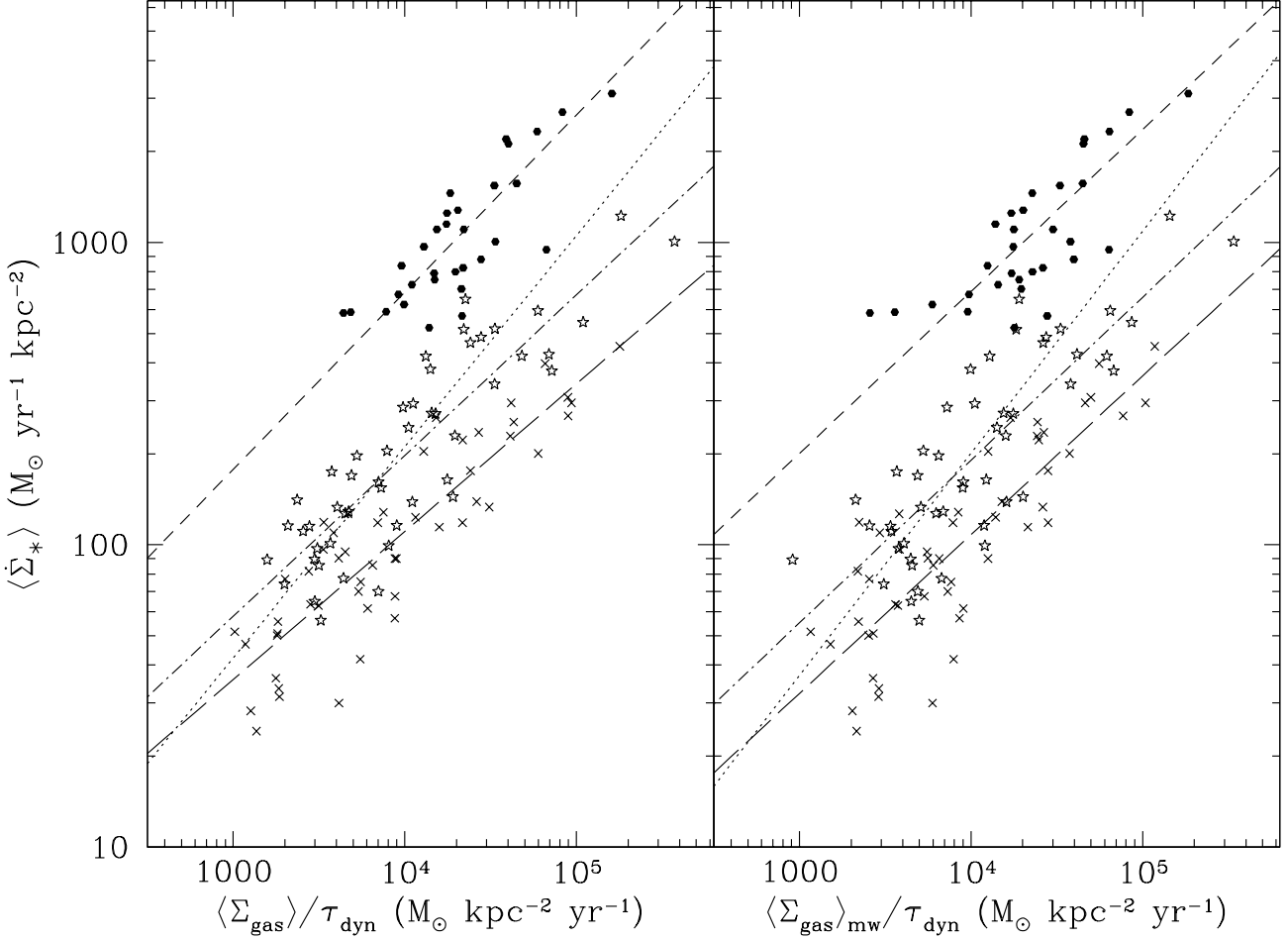
Figure 4. Elmegreen-Silk relations, defined either as $\langle \dot{\Sigma}_* \rangle$ vs. $\langle \Sigma_{\mathrm{gas}} \rangle / \tau_{\mathrm{dyn}}$ (left panel) or as $\langle \dot{\Sigma}_* \rangle$ vs. $\langle \Sigma_{\mathrm{gas}} \rangle_{mw} / \tau_{\mathrm{dyn}}$ (right panel), predicted by the Eddington-limited starburst disk models. The dynamical time, τ_{dyn}, is defined as the inverse of the orbital frequency at r_{out}, i.e., $\tau_{\mathrm{dyn}} = 1/\Omega(r_{\mathrm{out}})$. As for the KS laws (Fig. 3), the models are divided based on the multiplicitive dust-to-gas factor with the same symbol styles as the previous figure. When $\langle \dot{\Sigma}_* \rangle$ is plotted versus $\langle \Sigma_{\mathrm{gas}} \rangle / \tau_{\mathrm{dyn}}$ (left panel) the power-law slopes are equal to $n = 0.59$, 0.53 and 0.49 for a dust-to-gas enhancement of $1\times$, $5\times$ and $10\times$, respectively. If the $\langle \dot{\Sigma}_* \rangle$ is instead plotted against $\langle \Sigma_{\mathrm{gas}} \rangle_{mw} / \tau_{\mathrm{dyn}}$ (right panel) the slopes are $n = 0.54$, 0.54 and 0.53. The dotted line plots the least-squares fit to the all the points and has a slope of $n = 0.70$ (left panel) and 0.73 (right panel).

all the low J CO lines are fully thermalized and thus have approximately equal luminosities (see Armour & Ballantyne (2012) for example CO SLEDs from the radiation pressure dominated disks). As a result, neither the slope nor the scatter in the L_{TIR}-I_{CO} relationship depend significantly on the CO transition.

Interestingly, the slope of the L_{TIR}-I_{CO} relationship (1.1 ± 0.1) is very similar to the one predicted from the theoretical KS law ($N = 1.2$ or 1.3 when including all models; Fig. 3). However, this is purely a coincidence, because in these warm, dense and well-mixed disks both the dust and molecular gas emitters are thermalized, optically thick and represent the same amount of disk mass. Thus, a quasi-linear relationship between the L_{TIR} (indicating the dust mass) and I_{CO} (indicating the gas mass) is expected in this scenario (Krumholz & Thompson 2007). We conclude that L_{TIR}-I_{CO} plots are poor estimates of the star formation laws of radiation pressure dominated disks.

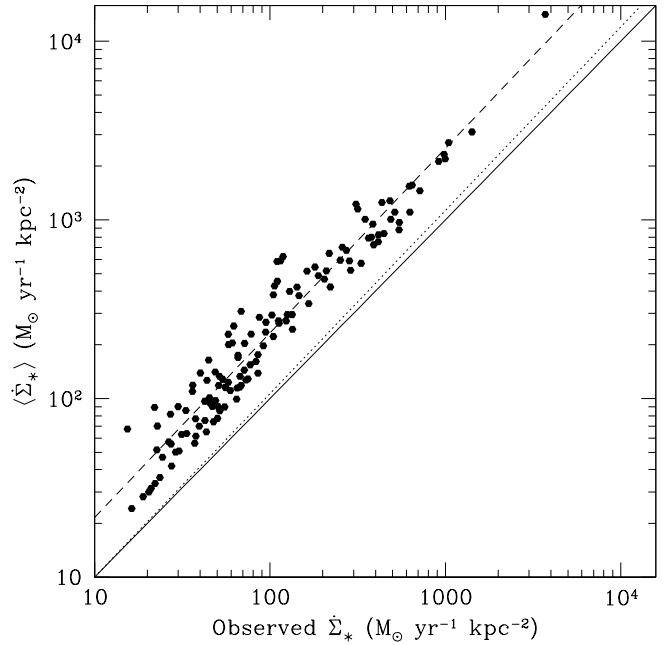The next step is to use the observables to estimate the physi-

cal quantities that enter into the star formation laws, beginning with $\dot{\Sigma}_*$. This quantity is reasonably straightforward to calculate, as one can simply translate the L_{TIR} into a SFR through one of the well known calibrations and then divide by the observed area of the disk to obtain the star formation surface density. Figure 6 illustrates how well that procedure recovers the actual $\langle \dot{\Sigma}_* \rangle$ of the model star-forming disks by plotting $\langle \dot{\Sigma}_* \rangle$ versus the values obtained from L_{TIR}, the relationship from Sect. 2.2, and the model inner and outer radii. The 'observed' $\dot{\Sigma}_*$ is highly correlated with $\langle \dot{\Sigma}_* \rangle$, and the least squares fit to the data (dashed line) has a slope of 1.04 ± 0.02, but is $\approx 2\times$ smaller than the one-to-one relationship. The dotted line is the least-squares fit to the model data if the Murphy et al. (2011) L_{TIR}-SFR relationship is used and results in a $\dot{\Sigma}_*$ that is approximately correct at low $\langle \dot{\Sigma}_* \rangle$, but becomes progressively too small at large $\langle \dot{\Sigma}_* \rangle$. These offsets from the actual $\langle \dot{\Sigma}_* \rangle$ is a result of approximating the average $\dot{\Sigma}_*$ with $(\langle \mathrm{SFR} \rangle)/\mathrm{area}$ or $(\mathrm{SFR}_{\mathrm{max}}/\mathrm{area})$, but are relatively
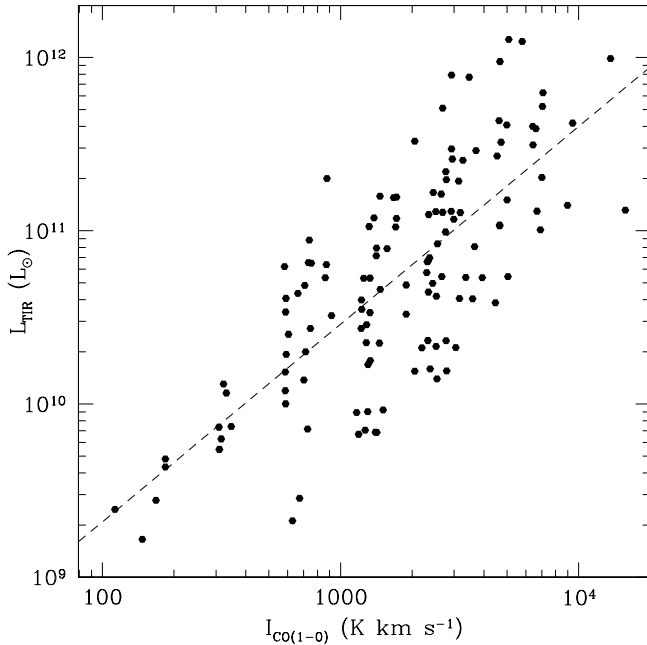
Figure 5. The L_{TIR} and I_{CO} relationship obtained from the Eddington-limited star-forming disk models. The dashed line shows the least-squares fit to the model data with a slope of 1.1 ± 0.1. If this plot is interpreted as an observational analogue of the KS law, then the slope is in reasonable agreement with the theoretical expectation of 1.2 or 1.3 (Fig. 3). However, this quasi-linear relation is simply a result of the molecular line and dust emission tracing the same gas population, and is not an accurate estimate of the underlying KS law.

Figure 6. A comparison between the $\langle \dot{\Sigma}_* \rangle$ predicted by the Eddington-limited starburst disks and the one calculated from the 'observed' L_{TIR}, a L_{TIR}-SFR correlation, and the inner and outer radii of the disk. The solid line plots the one-to-one correspondence between the two quantities, the dotted line is the relationship found when the Murphy et al. (2011) L_{TIR}-SFR calibration is used to derive $\langle \dot{\Sigma}_* \rangle$, while the data points and the dashed line result from the L_{TIR}-$\langle$SFR$\rangle$ correlation described in Sect. 2.2. This figure indicates that, due to the spatial variation of the star formation rate, any simple estimate of $\langle \dot{\Sigma}_* \rangle$ will be inaccurate by a factor of $\lesssim 2$.

minor. Most importantly, there is a good linear correlation between $\langle \dot{\Sigma}_* \rangle$ and the observational estimate, which indicates that the translation from L_{TIR} results in a reasonable estimate of $\langle \dot{\Sigma}_* \rangle$.

As described in Sect. 1 the conversion factor α_{CO} between I_{CO} and Σ_{gas} is not well determined except for a small number of galactic star-forming regions and some local ULIRGs (e.g., Downes & Solomon 1998; Solomon & Vanden Bout 2005; Narayanan et al. 2012). In our case, since we have both I_{CO} and $\langle \Sigma_{\mathrm{gas}} \rangle_{mw}$ for every model, we can calculate an unique value of α_{CO} for each star-forming disk (calculating α_{CO} with $\langle \Sigma_{\mathrm{gas}} \rangle$ instead of $\langle \Sigma_{\mathrm{gas}} \rangle_{mw}$ results in more scatter, so we focus on those computed with the mass-weighted average). Figure 7 plots the relationship between the resulting α_{CO} and I_{CO} and indeed finds a reasonable anti-correlation ($R = -0.64$, where R is the linear correlation coefficient) with a slope of -0.56 ± 0.06. The median value of α_{CO} is 3.56. As the CO intensity is correlated with the SFR (Fig. 5), this plot also indicates that α_{CO} is anti-correlated with the SFR. The slope of the α_{CO}-I_{CO} anti-correlation is steeper than the one of -0.32 found by Narayanan et al. (2012) from hydrodynamical simulations of galaxies. Similarly, the amplitude of the dotted line in Fig. 7 is $\gtrsim 2\times$ larger than the Narayanan et al. (2012) relation. As the physical scenario and calculation of the CO intensity performed by Narayanan et al. (2012) differs significantly from our setup the similarity in the results is striking. The relatively high gas temperatures found in the Eddington-limited star forming disks will tend to drive α_{CO} lower (Magnelli et al. 2012; Narayanan et al. 2012), which may explain the steeper slope in Fig. 7. The

larger amplitude may be caused by the lack of clumpiness in our star-forming medium which, when combined with the optically-thick nature of the CO emission, would result in the CO line intensity being a worse tracer of the total gas mass than in a clumpy medium where the CO intensity is directly related to a large number of smaller clouds. However, Papadopoulos et al. (2012) recently argued that the centers of ULIRGs (which may be radiation pressure dominated; Thompson et al. 2005) are unlikely to be comprised of individual molecular clouds and that the small values of α_{CO} inferred from these environments may be erroneously low, in agreement with the results presented in Fig. 7.

It is apparent from Fig. 7 that there is no single value of α_{CO} for a given I_{CO}; indeed, the scatter in α_{CO} at one I_{CO} can reach a factor of ten. Using the best-fit α_{CO}-I_{CO} relation will than propagate this large scatter through to the estimated Σ_{gas} (as seen in Fig. 8). The values of Σ_{gas} derived from α_{CO} are only weakly correlated ($R = 0.55$) with the $\langle \Sigma_{\mathrm{gas}} \rangle_{mw}$ calculated directly from the models. This poor relationship between I_{CO} and Σ_{gas} will substantially complicate any attempt to recover the star formation laws from the observational quantities.

Finally, Figure 9 presents the KS and ES laws of the radiation pressure supported star-forming disks derived solely from the observational quantities L_{TIR} and I_{CO}. To guide the analysis and comparison with the theoretical expectations (figs. 3 and 4), the models are separated by their dust-to-gas enhancement factor, although this may be impractical for a real observational sample. Recall that the Σ_{gas} computed from I_{CO}
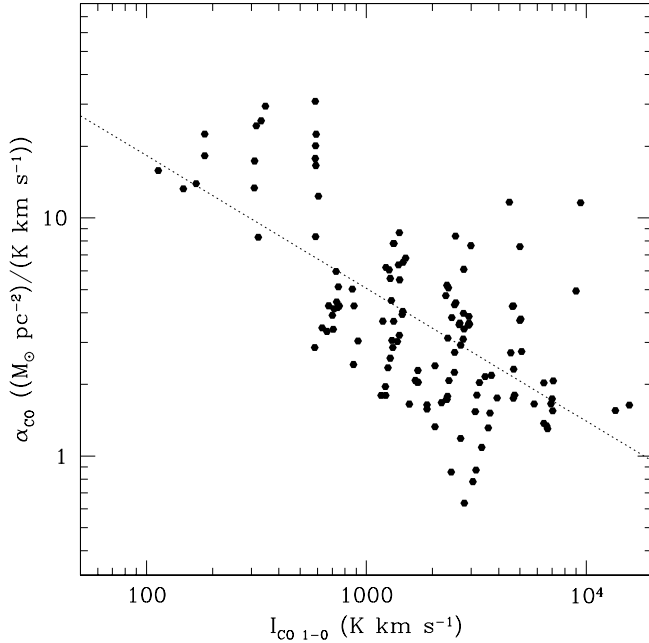
Figure 7. The relationship between $\alpha_{CO} = \langle \Sigma_{gas} \rangle_{mw}/I_{CO}$ and I_{CO} obtained from the radiation pressure dominated star-forming disks. The dotted line is the least-squares fit to the model data with a slope of -0.56 ± 0.06. As I_{CO} is correlated with the $\langle SFR \rangle$ (Fig. 5), this plot also shows that α_{CO} is anti-correlated with the $\langle SFR \rangle$.
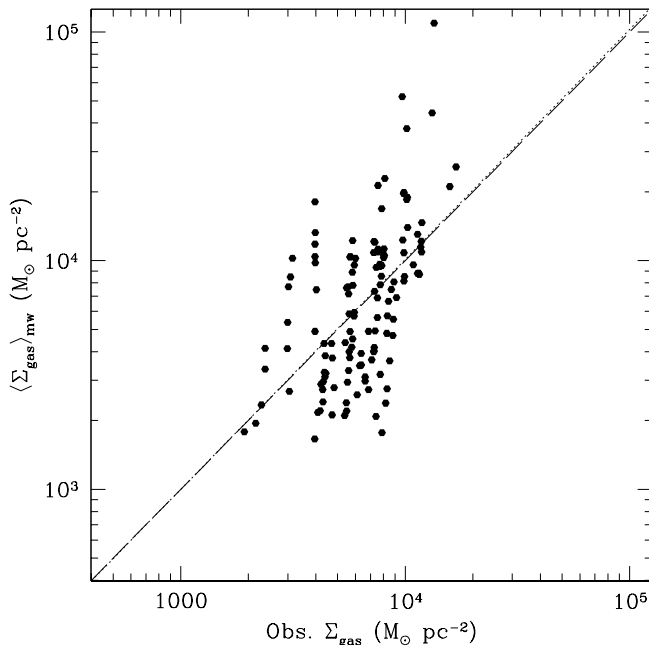
Figure 8. This figure compares the value of $\langle \Sigma_{gas} \rangle_{mw}$ derived directly from the star-forming disk models with those calculated from the 'observed' I_{CO} and the α_{CO}-I_{CO} relationship shown in Fig. 7. The long-dashed line is the one-to-one relationship and the dotted line is the least-squares fit to the data. While the two values agree on average, there is only a weak correlation ($r = 0.55$) between the $\langle \Sigma_{gas} \rangle_{mw}$ calculated from the model and the one derived from I_{CO}.

is an estimate of $\langle \Sigma_{gas} \rangle_{mw}$, so Fig. 9 should be compared to the right-hand panels of Figs. 3 and 4. As expected, the scatter of the 'observed' KS laws (rms$\approx$ 0.2) is larger than the ones found from the theoretical relations (rms$\approx$ 0.1). More striking are the differences in the correlation coefficient and slopes. The observationally derived KS laws have slopes of $N = 1.3 \pm 0.3$, 0.8 ± 0.2, and 0.5 ± 0.2 and correlation coefficients of $R = 0.6$, 0.5 and 0.4 as the dust-to-gas enhancement factor increases. In contrast the theoretically expected slopes are 0.94–1.0 and have correlation coefficients of > 0.9. Collecting all the models together yields a KS slope of $N = 1.4 \pm 0.2$ (with $R = 0.5$), surprisingly close to the canonical value, but, of course, yielding an entirely misleading view of the underlying physics. Thus, the KS law governing the Eddington-limited star-forming disks is nearly unrecognizable due to the very poor conversion between I_{CO} and Σ_{gas}. Our data indicate that the use of a higher density CO transition (such as CO $J = 3 - 2$) would not improve the conversion as this line is thermalized in these very warm disks. A high-J transition from a large density tracing molecule, such as HCN, may provide the best probe of Eddington-limited disks (although this needs to be confirmed by subsequent computations).

In contrast to the KS law, the 'observational' ES laws (right panel of Fig. 9) have similar correlation coefficients ($R \approx 0.8$) and about the same amount of scatter (rms$\approx$ 0.2) as the theoretically expected relations (right panel of Fig. 4). However, the slopes of the different ES laws are all $n > 0.7$, inconsistent with the expected slope of $n = 0.5$. The slope for the entire ensemble of models is $n = 1.2 \pm 0.1$, which, much like the KS law, leads to an erroneous description of the correct ES law. The steep slopes are a result of the uncertain α_{CO}-I_{CO} relation. If, for example, a constant $\alpha_{CO} = 3.56$, was used to estimate Σ_{gas}, then the slopes flatten to $n = 0.4$-0.7 for the individual dust-to-gas factors, and $n = 0.8 \pm 0.1$ when including all the models. These results are consistent with the theoretical ES law from Sect. 3.2. Applying this constant α_{CO} to the observed KS law results in a slope that is much too flat ($N = 0.2$–0.6). The slopes of the observed ES and KS relations are therefore very sensitive to the assumptions placed on α_{CO}; however, the low rms and large correlation coefficients found in the observed ES law are robust to the assumptions on α_{CO}, indicating that, out of these two relationships, the ES law may provide the most promising means to investigate SF laws at high redshift.

5. DISCUSSION & CONCLUSIONS

The purpose of this paper is to, one, elucidate the KS and ES laws of a Eddington-limited star-forming disk (including the impact of spatial averaging), and, two, to determine how well the theoretically expected star formation laws can be recovered by the standard conversions from the observables (L_{IR} and I_{CO}). To explore the effects of spatial averaging and how these disks might appear to telescopes, 1260 star-forming disk models, spanning a wide range of size and mass scales, were run to produce a bank of test data. From this model suite, 132 of the largest and most optically thick disks were selected to best describe the properties of Eddington-limited starbursts that may be embedded in the centers of the gas-rich star-forming galaxies.

The analytical model of a radiation pressure supported star-forming disk developed by Thompson et al. (2005) predicts a KS law with $N \approx 1$, and an ES law with $n \approx 0.5$, both significantly flatter than the canonical values ($N \approx 1.5$ and
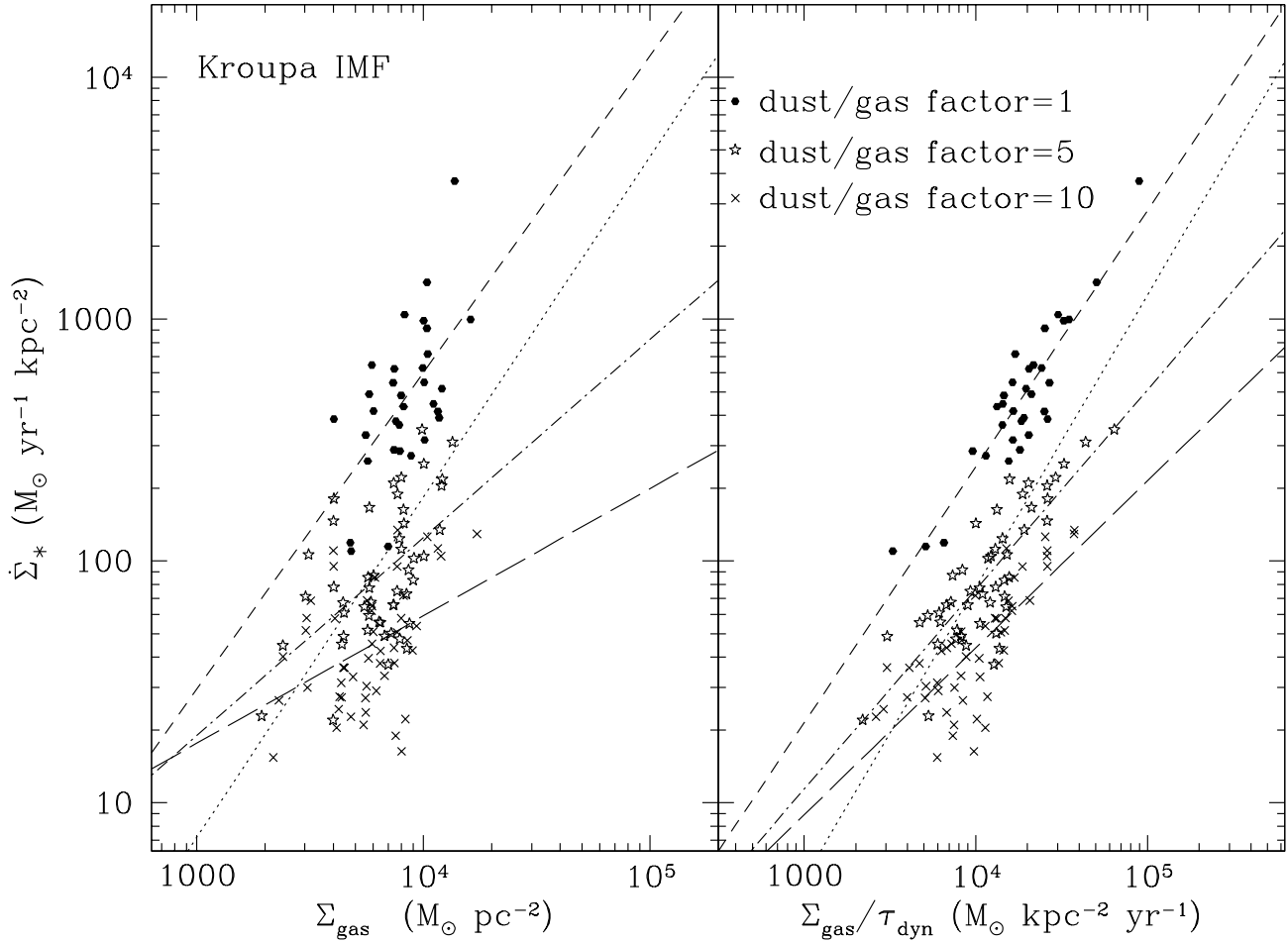
Figure 9. The KS (left panel) and ES (right-panel) laws of radiation pressure supported star-forming disks derived from the L_{TIR}-I_{CO} relationship (Fig. 5) as described in the text. As in the plots of the theoretically expected star formation laws (Figs. 3 and 4), the models have been separated by the value of the dust-to-gas enhancement factor. The slope of the relations are dependent on the dustiness of the gas with the KS relations yielding $N = 1.3, 0.8$ and 0.5 for a dust-to-gas enhancement of $1\times, 5\times$ and $10\times$, respectively. For the ES relations the slopes are $n = 1.1, 0.8$ and 0.7 as the dustiness of the gas increases. The dotted line in each panel plots the relation when all models are considered, irrespective of the dust-to-gas factor. In that case, $N = 1.4 \pm 0.2$ (KS law) and 1.2 ± 0.1 (ES law). Overall, the laws derived from observations are poor representations of the actual star formation relations that govern the disk.

$n \approx 1$). An important aspect of these star formation laws is the dependence on the opacity, or, equivalently, the dustiness of the star-forming gas. Indeed, the star formation process in a radiation supported disk strongly depends on the dust opacity (Thompson et al. 2005), and, when spatially averaged, can even impact the slopes of the observed star formation laws (Figs. 3 and 4). Another important effect of the gas opacity is the vertical separation of the star formation laws based on the dust-to-gas enhancement factor (Figs. 3 and 4). A heterogeneous sample of Eddington-limited star-forming disks may then appear to have a significantly steeper slope than what is governing the disks and would lead to the wrong conclusion about the underlying star formation relations.

To study how these disks might appear observationally, molecular line radiative transfer calculations were performed and CO line velocity-integrated intensities, I_{CO}, were derived for all 132 star-forming disk models. Combining these results with the infrared luminosity, L_{TIR}, calculated from the SED of each model, allowed a quantitative test of deriving the star formation laws from observational data. The

calculated L_{TIR} and I_{CO} are approximately linearly correlated with each other (albeit with a substantial scatter of rms= 0.4; Fig. 5), as might have been expected from the theoretical KS law. However, in the Eddington-limited star-forming disks, the gas density and temperature are always above the critical density and excitation temperature of the first several CO rotational transitions. These lines are therefore completely thermalized and are tracing the same gas as the infrared emission, resulting in a near-linear relationship (e.g., Krumholz & Thompson 2007; Narayanan et al. 2008). Indeed, the densities and temperatures of these disks are so large that a linear relationship is also expected for the low J transitions of molecules with higher critical densities (such as HCN or HCO$^+$), as seen in some ULIRGs (e.g., García-Burillo et al. 2012). While such a linear relationship may indicate that the star-forming region could be radiation-pressure dominated, it does not give any information on the underlying KS law (Krumholz & Thompson 2007). Observations of high-J transitions from these molecules may be needed to determine the KS and ES laws from the observed

IR luminosity and molecular line intensity.

If the $L_{\rm TIR}$-$I_{\rm CO}$ relation cannot be trusted as a measurement of the star formation laws of Eddington-limited disks, then these quantities must be translated to $\dot{\Sigma}_*$ and $\Sigma_{\rm gas}$. Figure 6 shows that the use of a $L_{\rm TIR}$-SFR conversion and the outer radius of the disk results in a $\langle \dot{\Sigma}_* \rangle$ that is within a factor of 2 of the correct value. On the other hand, $\alpha_{\rm CO}$, the phenomenological conversion factor between $I_{\rm CO}$ and $\Sigma_{\rm gas}$, exhibits significant scatter (about an order of magnitude for a given $I_{\rm CO}$; Fig. 7) and yields a very weak correlation between the estimated $\Sigma_{\rm gas}$ and the true $\langle \Sigma_{\rm gas} \rangle_{mw}$ (Fig. 8). This poor conversion from $I_{\rm CO}$ to $\Sigma_{\rm gas}$ causes the resulting KS laws (Fig. 9 (left)) to have only a weak correlation between $\dot{\Sigma}_*$ and $\Sigma_{\rm gas}$. The slopes of this KS relation vary strongly with the dustiness of the gas, reaching as low as $N = 0.5 \pm 0.2$ for a dust-to-gas factor of 10. The slope of $N = 1.4 \pm 0.2$ found from including all the models is consistent with the canonical slope, which perfectly illustrates how the observed KS law can distort and mislead the interpretation of star formation laws.

The situation is improved somewhat when considering the ES law, calculated by dividing the $I_{\rm CO}$-derived $\Sigma_{\rm gas}$ by the orbital time at $r_{\rm out}$ (Fig. 9 (right)). In this case, the observed ES laws retain the large correlation coefficients expected from the theoretical predictions, but, as with the KS law, the slopes are significantly steeper ($n > 0.7$) than what the theory predicts ($n \approx 0.5$). Similar to the KS law, the slope found from the ensemble of models ($n = 1.2 \pm 0.1$) is close to the canonical linear slope, leading to yet another erroneous conclusion about the underlying star formation law.

These experiments all point to the same problem: the $\alpha_{\rm CO}$ conversion factor is too blunt and inaccurate an instrument to study the star formation laws in radiation pressure dominated disks. In many ways this is unsurprising, as the $\alpha_{\rm CO}$ factor has only been shown to accurately trace $\Sigma_{\rm gas}$ in local Galactic molecular clouds up to $\Sigma_{\rm gas} \approx 100$ $M_\odot$ pc^{-2} (Kennicutt & Evans 2012). The Eddington-limited disks are at such high surface densities that the medium may not be accurately described as a series of molecular clouds, but rather a continuous structure with a near unity molecular fraction. In their study of the CO SLEDs from these disks, Armour & Ballantyne (2012) noted that in many ways the thermalized molecular emission from these disks acts like a stellar spectrum, with a SLED shape that depends on excitation temperature and a normalization that depends on the internal energy generation, i.e., star formation. Therefore, a large, massive disk may produce a similar $I_{\rm CO}$ as a smaller, less massive disk that has a larger $\langle$SFR$\rangle$ (due to, e.g., a larger opacity). The CO emission is largely immune to to the total gas mass in each disk, and therefore the $\alpha_{\rm CO}$ is a poor tracer of $\Sigma_{\rm gas}$. We do find that $\alpha_{\rm CO}$ is inversely related to $I_{\rm CO}$ and $\langle$SFR$\rangle$, in agreement with other authors (Narayanan et al. 2012), but with an amplitude $\approx 2\times$ larger. This may be an effect of the high density and uniform molecular medium of these disks (Papadopoulos et al. 2012), but this result should be checked with more realistic two- or three-dimensional simulations.

Given the difficulties in using $\alpha_{\rm CO}$, how can we make progress in studying star formation laws, especially when $\Sigma_{\rm gas} \gtrsim 10^4$ $M_\odot$ pc^{-2}? Clearly the traditional method of CO rotational lines will not be particularly useful in this regime, so observations should focus on molecular species with higher critical densities, such as HCN. Recent results using HCN ob-

servations of ULIRGs that reach into this high-$\Sigma_{\rm gas}$ range do give KS and ES slopes consistent with the theoretical expectation for Eddington-limited disks, suggesting that radiation pressure dominated regions may be playing a role in these sources (García-Burillo et al. 2012). Unfortunately, the conversion factor of HCN and other higher density tracers is as uncertain as $\alpha_{\rm CO}$. Observational campaigns focusing on measuring these conversion factors over as wide a range of $\Sigma_{\rm gas}$ as possible will be necessary in order to confidently apply them for ULIRGS and at high redshift where large gas surface densities will be more common. Interestingly, the ES law appears to be more robust to changes in opacity and maintains a strong correlation even with the use of $\alpha_{\rm CO}$ (although the slope is still incorrect). This result implies that, at least for the Eddington-limited star-forming disks studied here, measurements of the ES law will be more useful in determining the underlying star formation relations than the KS law. Finally, the star formation laws of radiation pressure dominated disks are strongly dependent on the gas opacity, causing a vertical separation in the KS and ES plots. Fitting a line through the models without controlling for the differences in the dust-to-gas ratio results in a much steeper slope than the underlying star formation law. Thus, future observational work at these values of $\Sigma_{\rm gas}$ would benefit from analyzing samples of galaxies with metallicity or dust-to-gas ratio estimates in order to control for this potentially misleading effect.

In summary, the KS and ES star formation laws for radiation pressure supported star-forming disks have flatter slopes ($N \approx 1$ and $n \approx 0.5$) than what is expected for star formation at $\Sigma_{\rm gas} \lesssim 10^4$ $M_\odot$ pc^{-2}. These slopes are relatively robust to spatial averaging over the disks, but the strong dependence on the opacity causes the relations to be vertically offset based on the dust-to-gas ratio. Thus, an erroneously large slope for the KS and ES laws could result if the opacity dependence is not recognized. Attempting to recover these star formation laws from the predicted $L_{\rm TIR}$ and $I_{\rm CO}$ failed because of the poor translation from $I_{\rm CO}$ to $\Sigma_{\rm gas}$ at these high densities and temperatures. The 'observed' KS and ES laws have slopes that differ significantly from the theoretically expected relations, even when controlling for the gas opacity. Progress in identifying and studying the star formation laws at these values of $\Sigma_{\rm gas}$ can be made by moving to well calibrated high critical density molecular tracer, selecting a sample of galaxies with metallicity estimates, and focusing on the ES relation, as its slope seems less affected by variations in metallicity and spatial averaging.

REFERENCES

Andrews, B.H. & Thompson, T.A., 2011, ApJ, 727, 97
Armour, J.N. & Ballantyne, D.R., 2012, ApJ, 752, 87
Ballantyne, D.R. 2008, ApJ, 685, 787
Calzetti, D., Wu, S.-Y., Hong, S. et al., 2010, ApJ, 714, 1256
Carilli, C.L. & Walter, F., 2013, ARA&A, in press (arXiv:1301.0371)
Daddi, E., Bournaud, F., Walter, F. et al., 2010a, ApJ, 713, 686
Daddi, E., Elbaz, D., Walter, F., et al., 2010b, ApJ, 714, L118
Diamond-Stanic, A.M., Moustakas, J., Tremonti, C.A., et al., 2012, ApJ, 755, L26
Downes, D. & Solomon, P.M., 1998, ApJ, 507, 615
Elmegreen, B.G., 1997, Rev. Mex. Astron. Astrofis. Conf. Ser., 6, 165
Elmegreen, B.G., ApJ, 577, 206
Englmaier P. & Shlosman I., 2004, ApJ, 617, L115
Feldmann, R., Gnedin, N.Y. & Kravtsov, A.V., 2012, ApJ, 758, 127

Freundlich, J., Combes, F., Tacconi, L.J. et al., 2013, A&A, in press (arXiv:1301.0628)
Gao, Y. & Solomon, P.M., 2004a, ApJS, 152, 63
Gao, Y. & Solomon, P.M., 2004b, ApJ, 606, 271
García-Burillo, S., Usero, A., Alonso-Herrero, A. et al., 2012, A&A, 539, A8
Geach, J.E., Smail, I., Moran, S.M., et al., 2011, ApJ, 730, 19
Genzel, R., Burkert, A., Bouché, N. et al., 2008, ApJ, 687, 59
Genzel, R., Tacconi, L.J., Gracia-Carpio, J., et al., 2010, MNRAS, 407, 2091
Goldsmith, P.F., 2001, ApJ, 557, 736
Goodman, J., 2003, MNRAS, 339, 937
Hogerheijde, M.R. & van der Tak, F.F.S, 2000, A&A, 362, 697
Hopkins, A.M. & Beacom, J.F., 2006, ApJ, 651, 142
Ivison, R.J., Papadopoulos, P.P., Smail, I., et al., 2011, MNRAS, 412, 1913
Klemperer, W., 2006, Proc. Natl. Acad. Sci. 103, 12232
Kennicutt, R.C.,Jr., 1998, ARA&A, 36, 189
Kennicutt, R.C.,Jr., 1998, ApJ, 498, 541
Kennicutt, R.C.,Jr., & Evans, N.J., 2012, ARA&A, 50, 531
Kroupa, P. & Weidner, C., 2003, ApJ, 598, 1076
Kroupa, P., Weidner, C., Pflamm-Altenburg, J., et al., 2012, in Stellar Systems and Galactic Structure, Vol V., Springer, in press (arXiv:1112.3340)
Krumholz, M.R. & McKee, C.F., 2005, ApJ, 498, 541
Krumholz, M.R., & Thompson, T.A., 2007, ApJ, 669, 289
Krumholz, M.R. & Thompson, T.A., 2012, ApJ, 760, 155
Krumholz, M.R., McKee, C.F. & Tumlinson, J., 2009, ApJ, 699, 850
Leitherer, C., Schaerer, D., Goldader, J.D., et al., 1999, ApJS, 123, 3
Maciejewski, W., 2004, MNRAS, 354, 892
Magdis, G.E., Daddi, E., Sargent, M., et al., 2012, ApJ, 758, L9
Magnelli, B., Saintonge, A., Lutz, D., et al., 2012, A&A, 548, A22
Muñoz-Mateos, J.C., Gil de Paz, A., Boissier, S., et al., 2009, ApJ, 701, 1965
Murray, N., Quataert, E. & Thompson, T., 2005, ApJ, 618, 569
Murphy, E.J., Condon, J.J., Schinnerer, E. et al., 2011, ApJ, 737, 67
Narayanan, D., Cox, T.J., Shirley, Y. et al., 2008, ApJ, 684, 996
Narayanan, D., Krumholz, M.R., Ostriker, E.C. & Hernquist, L., 2012, MNRAS, 421, 3127
Narayanan, D., Bothwell, M. & Davé, R., 2012b, MNRAS, in press (arXiv:1209.0771)
Ostriker, E.C. & Shetty, R., 2011, ApJ, 713, 41
Papadopoulos, P.P., van der Werf, P., Xilouris, E., Isaak, K.G. & Gua, Y., 2012, ApJ, 751, 10
Pelupessy, F.I., Papadopoulos, P.P. & van der Werf, P., 2006, ApJ, 645, 1024
Pérez-González, P.G., Rieke, G.H., Villar, V., et al., 2008, ApJ, 675, 234
Rieke, G.H., Alonso-Herrero, A., Weiner, B.J., et al., 2009, ApJ, 692, 556
Salpeter, E.E., 1955, ApJ, 121, 161
Sault, R.J., Teuben, P.J., & Wright, M.C.H. 1995. "A retrospective view of Miriad" In Astronomical Data Analysis Software and Systems IV. ed. Shaw, R., Payne, H.E., & Hayes, J.J.E. ASP Conference Series, 77, 433-436
Schmidt, M., 1959, ApJ, 129, 243
Semenov, D., Henning, Th., Helling, Ch., Ilgner, M. & Sedlmayr, E., 2003, A&A, 410, 611
Shetty, R. & Ostriker, E.C., 2012, ApJ, 754, 2
Silk, J., 1997, ApJ, 481, 703
Solomon, P.M. & Vanden Bout, P.A., 2005, ARA&A, 43, 677
Solomon, P.M., Downes, D., Radford, S.J.E. & Barrett, J.W., 1997, ApJ, 478, 144
Swinbank, A.M., Smail, I., Sobral, D., et al., 2012, ApJ, 760, 130
Tacconi, L.J., Genzel, R., Neri, R., et al., 2010, Nature, 463, 781
Thompson, T.A., 2009, in Wang W., Yang Z., Luo Z., Chen Z., eds, ASP Conf. Ser. Vol. 408, The Starburst-AGN Connection. Astron. Soc. Pac., San Francisco, p. 128
Thompson, T.A., Quataert, E., & Murray, N. 2005, ApJ, 630, 167
Tremaine, S., Gebhardt, K., Bender, R., et al., 2002, ApJ, 574, 740
Wisnioski, E., Glazebrook, K., Blake, C., et al., 2011, MNRAS, 417, 2601
Yao, L., Seaquist, E.R., Kuno, N. & Dunne, L., 2003, ApJ, 588, 771